ELSEVIER

Journal of Photochemistry and Photobiology A: Chemistry 143 (2001) 1–9

Journal of Photochemistry and Photobiology A:Chemistry

www.elsevier.com/locate/jphotochem

The temperature dependence (203–293 K) of the absorption cross sections of O_3 in the 230–850 nm region measured by Fourier-transform spectroscopy☆

S. Voigt, J. Orphal*, K. Bogumil, J.P. Burrows

Institut für Umweltphysik and Institut für Fernerkundung, Universität Bremen, P.O. Box 330440, D-28334 Bremen, Germany

Received 21 March 2001; received in revised form 14 May 2001; accepted 14 May 2001

Abstract

Absolute absorption cross sections of O_3 were measured in the 230–850 nm (11765–43478 cm^{-1}) region at five different temperatures (203–293 K) using a Fourier-transform spectrometer, at a spectral resolution of 5.0 cm^{-1} (corresponding to about 0.027 nm at 230 nm and to about 0.36 nm at 850 nm). The spectral accuracy of the data is better than 0.1 cm^{-1} — about 0.5 pm at 230 nm and about 7.2 pm at 850 nm — validated by recording of I_2 absorption spectra in the visible using the same experimental set-up. O_3 absorption spectra at different concentrations were recorded at five different sample temperatures in the range 203–293 K, and at each temperature at two total pressures (100 and 1000 mbar) using O_2/N_2 mixtures as buffer gas. Within the limits of experimental uncertainties, no influence of total pressure on the O_3 spectrum was observed in the entire spectral region, as expected from the short lifetimes of the upper electronic states of O_3. The temperature dependence of the O_3 absorption cross sections is particularly strong in the Huggins bands between 310 and 380 nm, as observed in previous studies. An empirical formula is used to model the temperature dependence of the O_3 absorption cross sections between 236 and 362 nm, a spectral region that is particularly important for atmospheric remote-sensing and for photochemical modelling.

Keywords: Ozone; Atmospheric remote-sensing; Photochemical modelling

1. Introduction

Ozone, O_3, is an important minor constituent of the Earth's atmosphere [1,2]. It plays a significant role in atmospheric radiative transfer and photochemistry [3,4]. For many years, atmospheric O_3 concentrations have been determined using UV–VIS spectroscopy [5,6]. For this purpose, a number of laboratory measurements of the absorption spectrum of O_3 have been reported in the past [7–43]. In spite of the number of studies, significant uncertainties in the UV–VIS absorption cross sections of O_3 still exist. In order to monitor small changes in the atmospheric O_3 concentrations, it is essential to know the absorption strength of this molecule to high accuracy.

In the last decade, a new generation of powerful satellite-borne UV–VIS–NIR spectrometers for atmospheric remote-sensing (e.g. GOME [44] and SCIAMACHY [45]) has been developed, that will be followed by many other similar instruments on different meteorological satellites. These instruments observe backscattered, reflected and transmitted light from the Earth's atmosphere, and measure simultaneously the entire spectral region between about 250–800 nm at medium or high spectral resolution (0.2–0.4 nm). Such experiments require precise reference spectra of O_3 and of many other atmospheric absorbers in this spectral region.

In order to provide these reference spectra, new O_3 absorption spectra were recorded using the GOME Flight-Model (GOME-FM) spectrometer in 1994–1995, in the entire region 230–800 nm at five different atmospheric temperatures in the range 202–293 K, as reported previously [43]. This data set has immediately been used in many remote-sensing and photochemical studies, although the spectral calibration of these cross sections is only accurate to about 0.03 nm, the limitations arising from the experimental set-up.

While the accuracy of the spectral wavelength calibration is not critical for many scientific applications, it is essential for the retrieval of atmospheric concentrations of O_3 and other constituents, such as NO_2, NO_3, OClO, BrO, SO_2, CH_2O, and ClO, from remote-sensing measurements

☆ Dedicated to the memory of Richard C.M. Learner.

* Corresponding author. Present address: Laboratoire de Photophysique Moléculaire, CNRS-Université de Paris-Sud, UPR 3361 Bât. 350, Centre d'Orsay, F-91405 Orsay, France. Tel.: +33-1-6915-7528; fax: +33-1-6915-7530.

E-mail address: johannes.orphal@ppm.u-psud.fr (J. Orphal).

1010-6030/01/$ – see front matter
PII: S1010-6030(01)00480-4

in the UV and visible. During the computer analysis of atmospheric spectra by the differential optical absorption spectroscopy (DOAS) technique [46], a non-linear wavelength fitting procedure ("shift and squeeze") is often applied in order to take into account systematic errors in the wavelength calibration. However, it is well established that additional fitting parameters lead to correlations between the retrieved atmospheric concentrations and to larger statistical uncertainties.

To resolve this issue, an impressive number of new laboratory spectra of NO_2 [47–50], O_2/O_4 [51–54], SO_2 [55,56], H_2O [57–59], BrO [60,61], and OClO [62] have been recorded in the past years using UV–VIS Fourier-transform spectroscopy (FTS). This experimental technique combines the advantages of high spectral resolution, of a well-known instrumental line shape, and of a linear wave number scale [63]. However, up to the present study, no temperature-dependent absorption spectra of the most important trace gas O_3 have been recorded in the UV–VIS spectral region using FTS. In order to address this deficit, we have performed laboratory measurements of O_3 spectra at five different temperatures in the range 203–293 K, with a Fourier-transform spectrometer suitable for use in the ultraviolet and visible spectral regions.

2. Experimental

2.1. Experimental set-up

Absorption spectra of O_3 at different temperatures were recorded using the high-resolution Fourier-transform spectrometer (Bruker IFS-120 HR) at the University of Bremen, Germany. The instrument has a maximum spectral resolution of $0.004\,cm^{-1}$ [64] and operates in the spectral range between 600 and $45{,}000\,cm^{-1}$, using different combinations of broad-band light sources, beamsplitters/combiners, and detectors. For all spectra used in the present study, the same interferometer configuration was used in order to guarantee an accurate spectral calibration.

A Xenon arc lamp (Osram XBO 150W/2) with a water-cooled elliptical mirror (Amko) or a quartz-tungsten-halogen lamp (Osram Xenophot HLX 64610) were used as broad-band light sources. The beamsplitter/combiner is made of UV-grade quartz. All mirrors in the set-up including those inside of the Bruker spectrometer are coated with a thin layer of MgF_2 in order to obtain a high reflectivity in the UV region. The wavenumber accuracy of the instrument was validated by recording absorption spectra of gaseous I_2 in the visible at a spectral resolution of $0.6\,cm^{-1}$ and found to be better than $0.1\,cm^{-1}$ (about 0.5 pm at 230 nm and about 7.2 pm at 850 nm) [56,65].

The light was coupled out of the spectrometer after the interferometer chamber, which was evacuated to about 0.03 mbar during the experiments (all wave numbers and wavelengths in this paper are, therefore, given for vacuum conditions). For recording spectra in the region 11,500–30,000 cm^{-1}, an Si diode detector was used. For the region between 20,000 and $33{,}000\,cm^{-1}$, a GaP diode detector replaced the Si diode; for the UV region between 30,000 and 45,000 cm^{-1}, a solar-blind UV diode was employed (see Fig. 1). The spectral resolution was limited to $5.0\,cm^{-1}$ (corresponding to about 0.027 nm at 230 nm and to about 0.36 nm at 850 nm) because no changes of the O_3 absorption spectrum

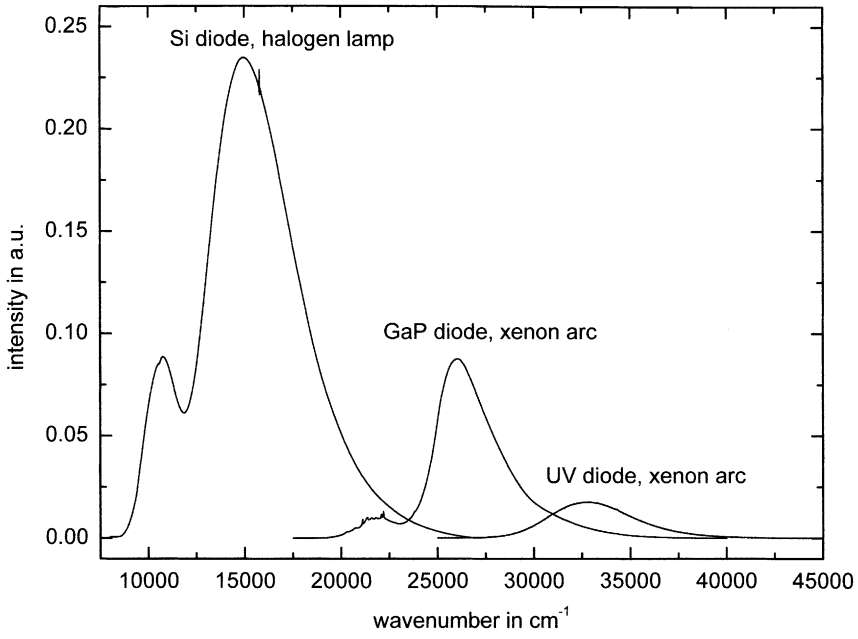

Fig. 1. Spectral distribution obtained using different white-light sources (Xenon arc, halogen lamp) and detectors (Si, GaP, and UV diodes) in order to cover the entire spectral region between 10,000 and $45{,}000\,cm^{-1}$ (225–1000 nm) with the FTS.

were observed at higher spectral resolutions. This restriction enabled us to achieve an optimal signal-to-noise ratio.

The absorption cell comprises a double-jacketed quartz vessel having a total length of 120 cm and an inner diameter of 5 cm. It can be equipped with a White-type mirror optics to achieve optical path lengths of up to 20 m. For the present study, spectra were recorded at optical path lengths of 120 cm (UV diode detector), of 505 cm (GaP diode detector), and of 985 cm (Si diode detector). Liquid ethanol flows through the inner jacket of the cell as a coolant, the outer jacket being evacuated for thermal insulation. In addition, the absorption cell was completely wrapped into black isolating foam (Armaflex) for additional thermal stability.

The temperature of the cell was controlled by a commercial two-stage cryogenic cooler (Haake KT-90) and calibrated with a Pt-100 temperature element inside the absorption cell both before and after the experiments. The stability of the temperature was always better than ± 1 K and the absolute accuracy of the temperature is estimated to ± 1 K from the calibration of the cell temperature against the temperature of the cooler [56,65]. Relative O_3 absorption spectra were recorded at temperatures of 203, 223, 246, 280, and 293 K, and at each temperature at total pressures of 100 and 1000 mbar using different $O_3/O_2/N_2$ mixtures. The O_3 partial pressures were always significantly smaller than those of the buffer gases O_2 and N_2. The pressure in the absorption cell was measured using calibrated capacitive pressure transducers (MKS Baratron).

The optical interface between the Fourier-transform spectrometer and the absorption cell comprises an off-axis parabolic mirror and a spherical mirror for the *f*-number conversion, and a small spherical mirror (placed in the focus of the off-axis parabolic mirror) that acted as a field lens to provide a maximum throughput. The latter arrangement was particularly important because the *f*-numbers of the Bruker FTS and of the absorption cell are rather different (about 6 and 60, respectively). The design of this interface was made using a ray-tracing program in order to make an optimum choice for the different optical components.

Gaseous O_3 was generated in a silent discharge using a commercial ozoniser (Innovatec) that produces up to 5% of O_3 in a silent discharge through a flow of O_2. Before entering the cell, the O_3/O_2 mixture was diluted with gaseous N_2. Constant flow rates of O_2 and N_2 were maintained by calibrated MKS flow controllers. Typically, flow rates were between 0.8 and 1.9 l min^{-1} for N_2 and 1.5–50 l h^{-1} for O_2. High-purity O_2 (4.8) and N_2 (5.0) gases were purchased from Messer Griesheim Germany. Absorption spectra were recorded at different mixing ratios of $O_3/O_2/N_2$ in order to obtain O_3 optical densities in the 0.1–1.0 range.

2.2. Experimental procedure, data reduction, and error analysis

Before and after recording O_3 absorption spectra at different total pressures, sample temperatures, and O_3 partial pressures, reference spectra of the white-light source were recorded in order to obtain an accurate zero-absorbance baseline. These spectra were used as reference to calculate weighted baseline spectra for the O_3 absorption spectra, which were recorded in blocks every 15 min. In this way, O_3 optical densities were obtained with weighted reference spectra and all blocks were averaged. The linearity of the lamp drifts, which were as large as 20% in the UV region, was validated with spectra of the empty absorption cell recorded under identical conditions [56,65].

The O_3 optical densities were finally scaled and concatenated at three different wave numbers, to take into account the different absorption in the Hartley, Huggins, and Chappuis bands of O_3, as well as the use of different detectors (see Fig. 1): at 33,000 cm^{-1} (303 nm), at 31,000 cm^{-1} (323 nm), and at 21,000 cm^{-1} (476 nm, for total pressures of 100 mbar) or 22,500 cm^{-1} (444 nm, for total pressures of 1000 mbar). The difference of the concatenation wavenumbers for 100 and 1000 mbar is explained by the differences in the O_3 optical densities that could be achieved at these total pressures.

To obtain absolute absorption cross sections in agreement with previous studies, we scaled the optical densities at each temperature to absolute cross sections using the integrated absorption cross sections of O_3 recorded using the GOME-FM spectrometer [43]. The advantages of using absorption cross sections integrated over the full width of an electronic band are (1) that they are — within the validity of the Born–Oppenheimer approximation — independent of the sample temperature (as observed for O_3 where the integrated values for the Hartley band have been shown to be independent of temperature to better than 1% by different authors [25–29,43]), and (2) that they are independent of the spectral resolution. We decided to use the integrated absorption cross sections recorded with the GOME-FM instrument because they cover the full spectral range 230–790 nm. If some other values for the UV–VIS O_3 cross sections should be recommended for general use in the future, it will be sufficient to re-scale the cross sections of this study by the same factor as those recorded with the GOME-FM instrument (at all temperatures). The absolute uncertainty of the O_3 absorption cross sections of the study carried out using the GOME-FM spectrometer is less than 3%. Additional uncertainties are due to the signal-to-noise ratio varying with the total pressure as a result of the different optical densities of O_3 in regions of small absorption cross sections, and also with the spectral region under consideration as a result of the white-light lamp spectral function. The absorption cross sections determined in this study also contain uncertainties due to residual baseline drifts depending on the spectral region; they are strongest in regions where the lamp signal is comparatively small (see Fig. 1). The total uncertainties of the absorption cross sections, therefore, depend both on the spectral region and on the total pressure.

Generally, the O_3 spectra at a total pressure of 1000 mbar have a better signal-to-noise ratio and less residual

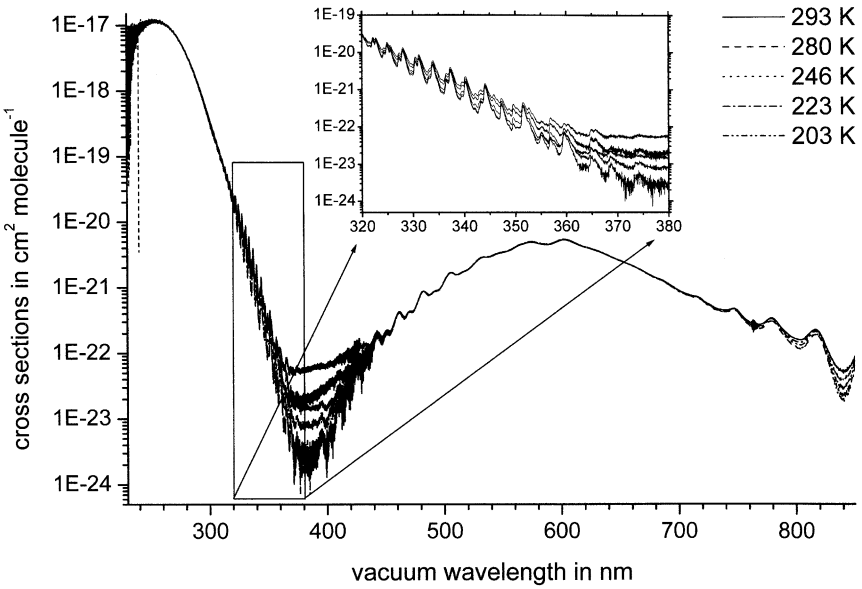

Fig. 2. The new O_3 absorption cross sections of this study at a spectral resolution of 5.0 cm^{-1}. Note the logarithmic scale of the ordinate since the cross sections vary over more than seven orders of magnitude. Note also the systematic decrease of absorption cross sections at lower temperatures in the region between 350 and 450 nm.

baseline errors. The smallest uncertainties are achieved in the regions below 21,000 cm^{-1} (3–6%) and between 28,500 and 37,000 cm^{-1} (4–7%). Above 37,000 cm^{-1}, the signal-to-noise ratio becomes smaller because of the decreasing lamp output in the UV, and between 21,000 and 28,500 cm^{-1} the O_3 absorption cross sections are small and result in a smaller signal-to-noise ratio and increasing uncertainties due to residual baseline errors.

It is important to stress the fact that the advantage of the accurate wavelength calibration is maintained over the entire spectral region between 230 and 850 nm, and that the error in the differential absorption cross sections (which are used for the analysis of atmospheric data) is small even in the case of systematic baseline drifts in regions of weak absorption, e.g. between 350 and 420 nm (see Fig. 2). For example, the new FTS O_3 absorption cross sections have already been used successfully to improve the spectral calibration of the O_3 spectra recorded with the GOME-FM [43].

In addition, the resolution (5.0 cm^{-1}) of the new spectra is significantly higher than those obtained by the grating spectrometers used for atmospheric remote-sensing (usually 0.4–1.0 nm, corresponding to 25.0–62.5 cm^{-1} at 25,000 cm^{-1}). The signal-to-noise ratio in regions of small absorption cross sections is better after convolution of the new FTS O_3 absorption cross sections with the instrumental line shapes of the atmospheric spectrometers. This improvement is well illustrated by the fact that different research groups who work on the retrieval of O_3 and other atmospheric constituents using ground-based atmospheric spectra already included the spectra of the present study in their data analysis, and reported improved results resulting from the high wavelength accuracy and from the good signal-to-noise ratio. This feature is of particular importance in the region 350–400 nm, where BrO and OClO features are present in atmospheric spectra under perturbed conditions [66].

3. Results and discussion

Within the limits of experimental accuracy, no pressure dependence of the O_3 absorption cross sections in the entire region 230–850 nm was observed; i.e. the only differences are due to noise and baseline changes. This result is in agreement with expectations from the upper state's lifetime, because all excited electronic states of O_3 leading to the absorption spectrum between 230 and 850 nm are repulsive or highly predissociated. The only region where a possible pressure dependence could have been expected is between 310 and 380 nm (the Huggins bands, see inset in Fig. 2). However, no rotational lines are observable in these bands, illustrating that rapid predissociation is predominant in this system. It is interesting to note that a recent study [67] of the atomic O ^1D quantum yields from O_3 photolysis in the region between 315 and 375 nm (which is a spin-forbidden process) concluded that the cross sections of the present study lead to more consistent results than other O_3 absorption cross sections published previously.

While the integrated absorption cross sections of O_3 were assumed to be constant, there are regions with a clear temperature dependence of the absorption cross sections which is strongest in the Huggins bands between 310 and 380 nm (see Fig. 3), in agreement with previous studies of the O_3 cross sections in this region [25–29]. The

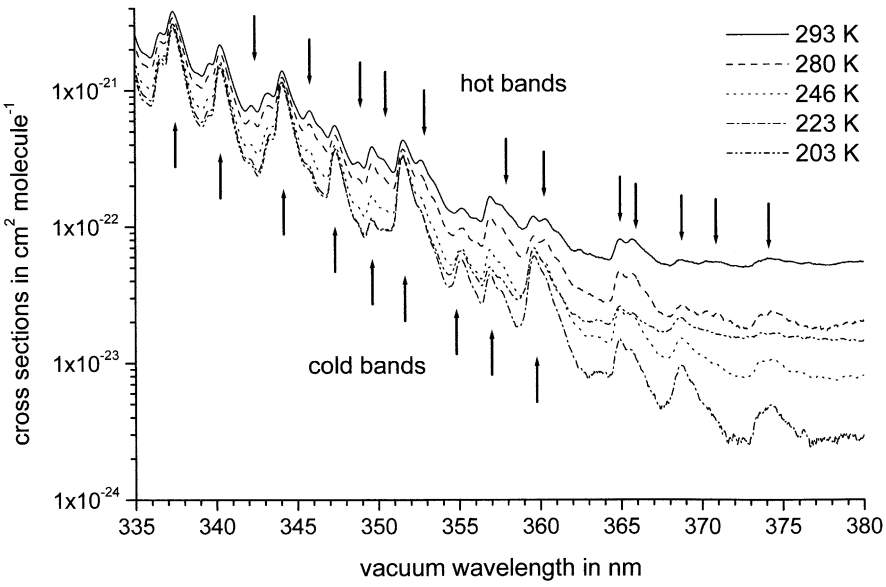

Fig. 3. The temperature-dependent absorption cross sections in the Huggins bands clearly show the presence of "hot bands" arising from excited vibrational levels in the electronic ground state, leading to changes in the differential cross sections with temperature. At the same time, this region is influenced by the slope of the Hartley band, leading to an increase of the absolute absorption cross sections with increasing temperature.

temperature dependence of transitions arising from excited vibrational states — (1 0 0), (0 0 1), and (0 1 0) — in the electronic ground state ("hot bands") is shown in Fig. 3, in good agreement with previous work [68–72]. Vibrational assignments of the Huggins bands lead to a set of improved vibrational constants for the upper electronic state. These data, determined from a linear least-squares fit of the band centres to a Dunham-type expansion, are shown in Table 1. Note that it is still impossible to determine the symmetry of the upper electronic state from these assignments, so that future experimental and theoretical work is required to resolve this issue. However, independent of the theoretical analysis, the influence of the "hot bands" is very important for the analysis of atmospheric spectra in this region, as demonstrated by the differential cross sections in Fig. 4.

Table 1
Spectroscopic parameters of the Huggins bands of O_3[a]

Constant	This work	[72]	[68]	[71]
T_e	26126 (14)	–[b]	26139 (12)	26120 (12)
ω_1	753.2 (43)	743.5	762.5 (23)	762.3 (34)
$\omega_2 + x_{22}$	410.6 (80)	440.6	407.4 (113)	409.4 (118)
ω_3	788.0 (63)	800.2	833.4 (82)	798.7 (38)
x_{11}	16.8 (4)	23.4	19.0 (4)	19.0 (6)
x_{12}	22.2 (16)	24.4	18.8 (22)	18.8 (30)
x_{13}	37.2 (7)	28.1	37.0 (16)	37.5 (12)
x_{23}	21.0 (20)	11.5	27.2 (84)	23.0 (34)
x_{33}	18.0 (8)	13.4	21.8 (39)	19.5 (8)
rms	7.2	–[b]	6.8	6.8

[a] Numbers in parentheses indicate the standard deviation (1σ) in units of the last digit.

[b] These values are not given in the paper [72] that describes theoretical work.

At lower temperatures, the cold bands become more pronounced, leading to an increase of their differential cross sections with decreasing temperature, while the "hot bands" disappear (leading to a decrease of the differential cross sections) with decreasing temperature at such wavelengths.

An important temperature effect is also observed on the blue wing of the Chappuis band between 400 and 500 nm. In this region, the overall magnitude of the cross sections decreases with lower temperatures (see Fig. 2), and the differential cross sections also change with temperature (see Fig. 5), in good agreement with the study of Burkholder and Talukdar [41] and with our previous work using the GOME-FM instrument [43]. Note that the shift of the peak positions of the differential cross sections towards smaller wavelengths with decreasing temperatures (nearly 0.2 nm between 293 and 203 K) already observed in the spectra recorded with the GOME-FM instrument is clearly confirmed by the new FTS data. This shift is particularly important for the analysis of atmospheric spectra and requires further theoretical investigation. The slight increase of the differential cross sections at the top of the Hartley band (ca. 240–270 nm) is also in agreement with several previous studies [25–29].

The O_3 cross sections at different temperatures in the region between 350 and 420 nm show an overall decrease with temperature except at the lowest value, 203 K. Although it cannot be entirely excluded that a baseline error is responsible for this observation, the same effect was observed qualitatively in the spectra recorded with the GOME-FM instrument [43] and in recent measurements using the SCIAMACHY-PFM instrument [73]. Because high-purity gases were used, contributions from gaseous

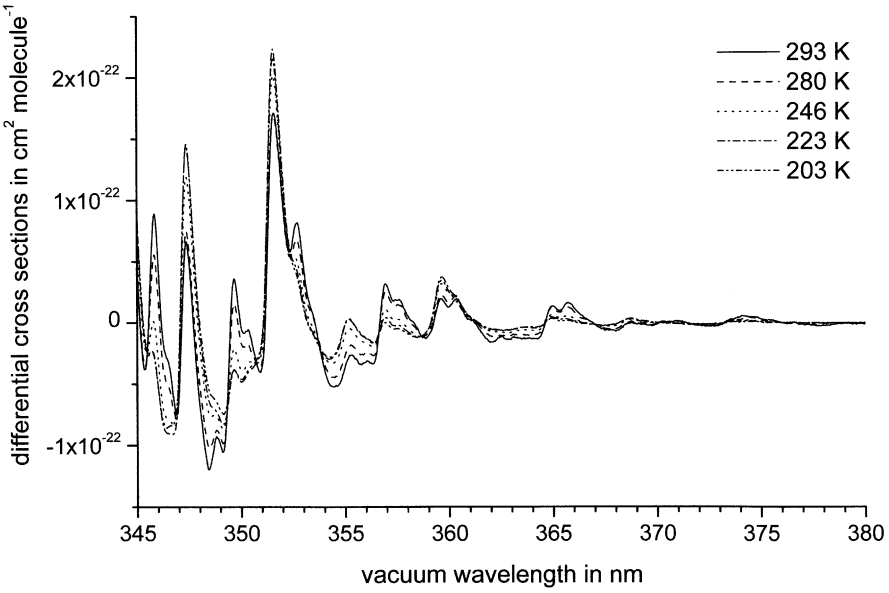

Fig. 4. Temperature dependence of the differential absorption cross sections in the Huggins bands between 345 and 380 nm, a spectral region which is currently used for measuring OClO and BrO in the atmosphere. Note the different behaviour for cold and "hot" bands, and the good signal-to-noise ratio in the entire region.

impurities are not expected in this region, and the increased absorption at low temperatures could not be identified with a known molecular absorber, such as O_4, NO_2, N_2O_3, N_2O_4, HONO, etc. Although the physical reason for the observed effect is unclear (a possible explanation could be the formation of a weakly-bound molecular complex of O_3 and O_2 at lower temperatures), this increase of the O_3 cross sections with decreasing temperature in the near-ultraviolet would be of great importance for atmospheric photochemistry. Obviously further experimental effort is required to elucidate this question.

In order to calculate absorption cross sections at intermediate temperatures (in view of the atmospheric remote-sensing applications often using more than five atmospheric layers) and to reduce systematic uncertainties due to residual baseline errors, an empirical three-parameter model was

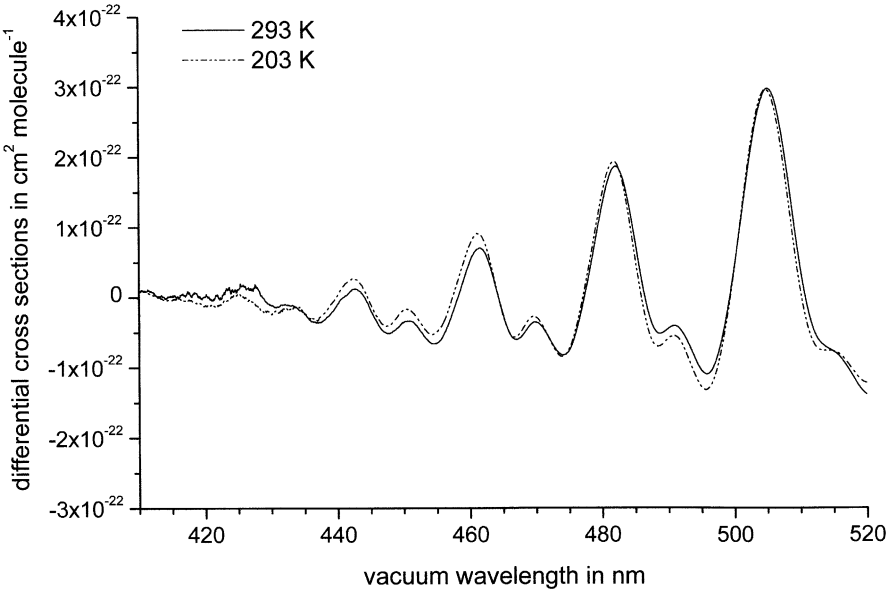

Fig. 5. Temperature dependence of the differential absorption cross sections in the blue wing of the Chappuis band between 415 and 520 nm. This spectral region is used for ground-based measurements of O_3 and NO_2 from zenith-sky spectra. Note the slight increase of the differential absorption cross sections with decreasing temperature, and the clear shift of the peaks towards smaller wavelengths (nearly 0.2 nm between 293 and 203 K).

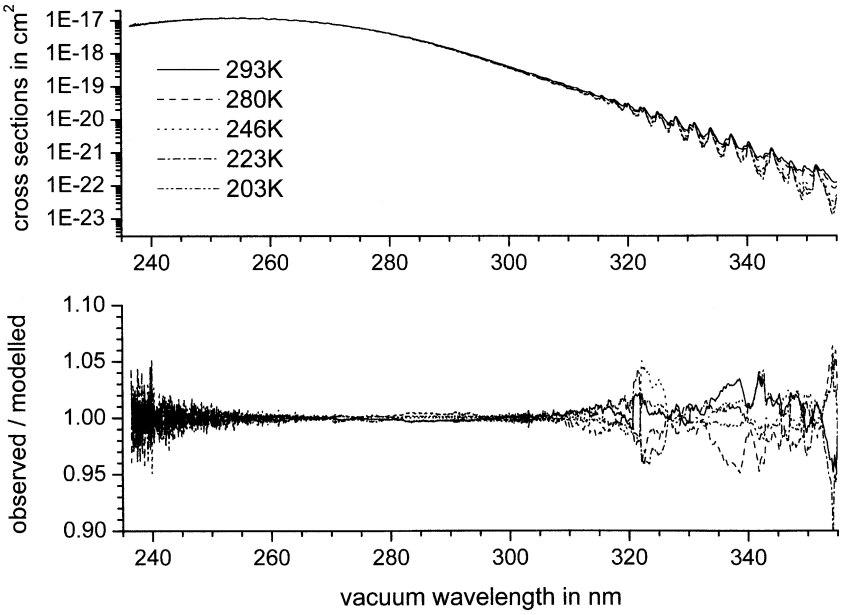

Fig. 6. Upper trace: temperature dependence of the O_3 absorption cross sections in the region 236–355 nm as reproduced by a three-parameter model (see text for details). Lower trace: the ratio of measured to the modeled cross sections shows noise up to 5% in the region below 260 nm, and systematic errors in the measured cross sections above 320 nm mainly due to residual baseline drifts.

used to reproduce the observed variation of the O_3 absorption cross sections as a function of temperature, at all wavelengths between 236 and 362 nm (a spectral region that is particularly important for atmospheric remote-sensing and for photochemical modelling). The model uses a constant and two exponential functions with a temperature-dependent exponent

$$\sigma(\lambda, T) = \exp\left[\frac{Tx_1(\lambda) - x_2(\lambda)}{T} - x_3(\lambda)T\right]$$

with three wavelength-dependent parameters $x_1(\lambda)$, $x_2(\lambda)$, and $x_3(\lambda)$ that were adjusted by a non-linear least-squares fitting routine to reproduce the observed data at each wavelength λ. The agreement between observed and modelled data is very good (see Fig. 6), i.e. 1% and better in the region 255–310 nm, up to 5% at smaller wavelengths (due to noise in the observed data), and up to 10% above 355 nm (probably due to baseline errors in the observed data). From Fig. 6, it becomes clear that systematic errors in the vicinity of concatenating wavelengths are reduced by the model, because they appear in the residuals. At the same time, one can see the increased signal-to-noise ratio compared to Fig. 1 (note that the model was calculated using the original data convoluted with a 20 cm^{-1} FWHM Gaussian function). The interpretation of the three wavelength-dependent parameters $x_1(\lambda)$, $x_2(\lambda)$, and $x_3(\lambda)$ needs further theoretical investigation.

A general comparison of the O_3 absorption cross sections and their temperature dependence in the 230–850 nm region is currently being prepared, using all previously published data [7–42] including the GOME-FM spectra [43] and the results of the present work, and additionally new absorption spectra recorded in 1998–1999 using the SCIAMACHY satellite spectrometer prior to launch [73]. A first comparison of the new data of this study with previous work is given in Tables 2 and 3, showing that the cross sections of this study at room temperature for selected wavelengths are in good agreement with those from previous work. It is important to stress the fact that using this new data set for atmospheric remote-sensing applications represents an important experimental validation. Potential users are,

Table 2
Absorption cross sections of O_3 at 293 K in the Hartley and Huggins bands (in units of 10^{-20} cm^2)

Wavelength (nm)	This work	Hearn [15]	Bass and Paur [28]	Molina and Molina [29]	Daumont et al. [25]	Mauersberger et al. [31]	Yoshino et al. [39]	Burrows et al. [43]
253.65	1137	1147	1145	1157	1130.5	1136	1143	1150
289.36	154	147	150	154	151	–	149	153
296.73	61.7	59.7	61.1	62.3	61.5	–	59.7	61.9
302.15	30.4	28.6	29.8	30.3	29.9	–	29.1	30.2
334.15	0.0509	0.0430	0.0470	0.0446	0.0466	–	0.0437	0.0494

Table 3
Absorption cross sections of O_3 at 293 K in the Chappuis band (in units of 10^{-23} cm^2)

Wavelength (nm)	This work	Hearn [15]	Brion et al. [42]	Burkholder and Talukdar [41]	Anderson and Mauersberger [36]	Burrows et al. [43]
543.52	315	–	312	308	308	317
576.96	483	476	477	466	–	484
594.09	475	–	468	464	457	474
632.82	347	–	339	331	338	351

therefore, encouraged to undertake systematic comparisons of different O_3 reference spectra for atmospheric retrieval and to make their observations available.

4. Conclusion

The new absorption cross sections at different temperatures are an important contribution to our knowledge of the UV–VIS–NIR spectrum of O_3, in particular, because of the high wavelength accuracy and spectral resolution over the entire 230–850 nm region which has — to the best of our knowledge — not been achieved before. Comparisons with previous studies show general agreement concerning the temperature dependence of the O_3 cross sections, while a detailed quantitative analysis is currently in progress. The theoretical interpretation of the UV–VIS absorption cross sections of O_3 is, however, incomplete, and even with the most powerful ab initio methods it remains impossible to model the electronic absorption spectrum of O_3 within the experimental uncertainties. This difficulty underlines the need of accurate laboratory spectroscopy of O_3.

All data of this study are available in digital form on the WWW at the URL http://www.iup.physik.uni-bremen.de/gruppen/molspec/index.html and upon request to the authors.

Acknowledgements

This study was partly supported by the European Space Agency ESA-ESTEC under contract no. 11340/95/NL/CN, by the German Space Agency DARA/DLR under contract no. 50/EP/9207, and by the University of Bremen. The authors wish to thank J.W. Brault (Boulder, USA), A.P. Thorne and R.P. Learner (London, UK) for their suggestions about FT–UV spectroscopy, and M. Birk and G. Wagner (Oberpfaffenhofen, Germany) for a ray-tracing software of the Bruker IFS-120 HR spectrometer optics. We are much indebted to J. Brion, J. Malicet, A. Chakir, D. Charbonnier, and J. Daumont (Reims, France) for sending us publications and digital data, to D. Bauer (Miami, USA) for sending us a manuscript prior to publication, and to A. Richter (Bremen, Germany) for many discussions on atmospheric remote-sensing in the UV and visible. The excellent technical support of Bruker Germany GmbH (A. Keens, N. Schulz, and G. Surawicz) merits particular mention. J.O. thanks the Deutsche Forschungsgemeinschaft (DFG) for a research fellowship in the new Emmy-Noether program.

References

[1] R.P. Wayne, Chemistry of Atmospheres, 3rd Edition, Oxford University Press, Oxford, 2000.
[2] World Meteorological Organisation, Scientific Assessment of Ozone Depletion: 1998, WMO Global Ozone Research and Monitoring Project Report 44, Geneva, 1999.
[3] G. Brasseur, S. Solomon, Aeronomy of the Middle Atmosphere, Reidel, Dordrecht, 1986 (reprinted in 1995).
[4] B.J. Finlayson-Pitts, J.N. Pitts, Jr., Atmospheric Chemistry, Wiley, New York, 1986.
[5] W.B. Grant (Ed.), Ozone Measuring Instruments for the Stratosphere, Vol. 1, Collected Works in Optics, Optical Society of America, Washington, DC, 1989.
[6] R.E. Huffmann, Atmospheric Ultraviolet Remote-Sensing, Vol. 52, International Geophysics Series, Academic Press, San Diego, 1992.
[7] J. Chappuis, C. R. Acad. Sci. 91 (1880) 985.
[8] J. Chappuis, C. R. Acad. Sci. 94 (1882) 858.
[9] G.L. Humphrey, R.M. Badger, J. Phys. Chem. 15 (1947) 794.
[10] A. Vassy, E. Vassy, J. Chem. Phys. 16 (1948) 1163.
[11] L. Lefebvre, C. R. Acad. Sci. 200 (1953) 653.
[12] E. Vigroux, Ann. Phys. Paris 8 (1953) 709.
[13] E.C.Y. Inn, Y. Tanaka, J. Opt. Soc. Am. 43 (1953) 870.
[14] Y. Tanaka, E.C.Y. Inn, K. Watanabe, J. Chem. Phys. 21 (1953) 1651.
[15] A.G. Hearn, Proc. Phys. Soc. London 78 (1961) 933.
[16] W.B. DeMore, O. Raper, J. Phys. Chem. 68 (1964) 412.
[17] E. Vigroux, Ann. Phys. 2 (1967) 209.
[18] M. Griggs, J. Chem. Phys. 49 (1968) 857.
[19] R.D. Hudson, Rev. Geophys. 9 (1971) 305.
[20] R.D. Hudson, Can. J. Chem. 52 (1974) 1465.
[21] J.C.D. Brand, K.J. Cross, A.R. Hoy, Can. J. Phys. 56 (1977) 327.
[22] C.M. Penney, NASA Contract Report 158977, 1979.
[23] K.F. Klenk, Appl. Opt. 19 (1980) 236.
[24] D.E. Freeman, K. Yoshino, J.R. Esmond, W.H. Parkinson, Planet Space Sci. 32 (1984) 239.
[25] D. Daumont, J. Brion, J. Malicet, Planet Space Sci. 31 (1983) 1229.
[26] J. Brion, D. Daumont, J. Malicet, J. Phys. Lett. Orsay Fr. 45 (1984) 57.
[27] A.M. Bass, R.J. Paur, in: C. Zerefos, A. Ghazi, D. Reidel (Eds.), Proceedings of the Quadrennial Ozone Symposium, Halkidiki, Greece, 1985, p. 606.
[28] R.J. Paur, A.M. Bass, in: C. Zerefos, A. Ghazi (Eds.), Proceedings of the Quadrennial Ozone Symposium, Halkidiki, Greece,1985, p. 611.
[29] L.T. Molina, M.J. Molina, J. Geophys. Res. D 91 (1986) 14501.
[30] K. Mauersberger, J. Barnes, D. Hanson, J. Morton, Geophys. Res. Lett. 13 (1986) 671.
[31] K. Mauersberger, D. Hanson, J. Barnes, J. Morton, J. Geophys. Res. D 92 (1987) 8480.
[32] J. Barnes, K. Mauersberger, J. Geophys. Res. D 92 (1987) 14861.

[33] M. Cacciani, A. Di Sarra, G. Fiocco, A. Amoruso, J. Geophys. Res. D 94 (1989) 8485.
[34] D. Daumont, A. Barbe, J. Brion, J. Malicet, in: R.D. Bojkov, P. Fabian, A. Deepak (Eds.), Proceedings of the Quadrennial Ozone Symposium, Hampton, VA, 1989, p. 710.
[35] A. Amoruso, M. Cacciani, A. Di Sarri, G. Fiocco, J. Geophys. Res. D 95 (1990) 20565.
[36] S.M. Anderson, K. Mauersberger, Geophys. Res. Lett. 19 (1992) 933.
[37] D. Daumont, J. Brion, J. Charbonnier, J. Malicet, Atmos. Chem. 15 (1992) 145.
[38] J. Brion, A. Chakir, D. Daumont, J. Malicet, C. Parisse, Chem. Phys. Lett. 213 (1993) 610.
[39] K. Yoshino, J.R. Esmond, D.E. Freeman, W.H. Parkinson, J. Geophys. Res. D 98 (1993) 5205.
[40] W.D. Komhyr, C.L. Mateer, R.D. Hudson, J. Geophys. Res. D 98 (1993) 20451.
[41] J.B. Burkholder, R.K. Talukdar, Geophys. Res. Lett. 21 (1994) 581.
[42] J. Brion, A. Chakir, J. Charbonnier, D. Daumont, C. Parisse, J. Malicet, J. Atmos. Chem. 30 (1998) 291.
[43] J.P. Burrows, A. Richter, A. Dehn, B. Deters, S. Himmelmann, S. Voigt, J. Orphal, J. Quant. Spectrosc. Rad. Transfer 61 (1999) 509.
[44] J.P. Burrows, M. Weber, M. Buchwitz, V. Rozanov, A. Ladstaetter-Weissen-mayer, A. Richter, D. DeBeek, R. Hoogen, K. Bramstedt, K.-U. Eichmann, M. Eisinger, J. Atmos. Sci. 56 (1999) 151.
[45] H. Bovensmann, J.P. Burrows, M. Buchwitz, J. Frerick, S. Noel, V. Rozanov, K.V. Chance, A.P.H. Goede, J. Atmos. Sci. 56 (1999) 127.
[46] U. Platt, D. Perner, J. Geophys. Res. 85 (1980) 7453.
[47] G.J. Frost, L.M. Gross, V. Vaida, J. Geophys. Res. D 101 (1996) 3869.
[48] J.W. Harder, J.W. Brault, P.V. Johnston, G.H. Mount, J. Geophys. Res. D 102 (1997) 3861.
[49] A.C. Vandaele, C. Hermans, P.C. Simon, M. Van Roozendal, J.M. Guilmot, M. Carleer, R. Colin, J. Atmos. Chem. 25 (1996) 289.
[50] A.C. Vandaele, C. Hermans, P.C. Simon, M. Carleer, R. Colin, S. Fally, M.-F. Mérienne, A. Jenouvier, B. Coquart, J. Quant. Spectrosc. Radiat. Transfer 59 (1998) 171.
[51] D.A. Newnham, J. Ballard, J. Geophys. Res. D 103 (1998) 28801.
[52] P. Bernath, M. Carleer, S. Fally, A. Jenouvrier, A.C. Vandaele, C. Hermans, M.-F. Mérienne, R. Colin, Chem. Phys. Lett. 297 (1998) 293.
[53] R. Schermaul, R.C.M. Learner, J. Quant. Spectrosc. Radiat. Transfer 61 (1999) 781.
[54] R. Schermaul, J. Quant. Spectrosc. Radiat. Transfer 62 (1999) 181.
[55] A.C. Vandaele, P.C. Simon, J.M. Guilmont, M. Carleer, R. Colin, J. Geophys. Res. D 99 (1994) 25599.
[56] J. Ballard, D. Newnham, J. Orphal, S. Voigt, R. Learner, A. Thorne, M. Wickett, A Study of Absorption Cross Sections in the UV and Visible, Contract Report to ESA, prepared by Serco Ltd., London, 1998.
[57] J.W. Harder, J.W. Brault, J. Geophys. Res. D 102 (1997) 6245.
[58] M. Carleer, A. Jenouvrier, A.C. Vandaele, P.F. Bernath, M.-F. Mérienne, R. Colin, N.F. Zobov, O.L. Polyansky, J. Tennyson, V.A. Savin, J. Chem. Phys. 111 (1999) 2444.
[59] D.A. Newnham, Measurement of H_2O Absorption Cross Sections for the Exploitation of GOME Data, Progress Report 1, ESA Contract Report, prepared by Serco Ltd., London, 1999.
[60] D.M. Wilmouth, T.F. Hanisco, N.M. Donahue, J.G. Anderson, J. Phys. Chem. A 103 (1999) 8935.
[61] O.C. Fleischmann, J. Orphal, J.P. Burrows, in preparation.
[62] H. Kromminga, J. Orphal, J.P. Burrows, Phys. Chem. Chem. Phys. (2001), in preparation.
[63] P.R. Griffiths, J.A. de Haseth, Fourier-Transform Infrared Spectrometry, Wiley, New York, 1986.
[64] S. Voigt, S. Dreher, J. Orphal, J.P. Burrows, J. Mol. Spectrosc. 180 (1996) 359.
[65] S. Voigt, Ph.D. Thesis, University of Bremen, 1998.
[66] THESEO BrO Workshop, University of Bremen, 1999.
[67] D. Bauer, L. D'Ottone, A.J. Hynes, Phys. Chem. Chem. Phys. 2 (2000) 1421.
[68] D.H. Katayama, J. Chem. Phys. 71 (1979) 815.
[69] D.H. Katayama, J. Chem. Phys. 85 (1986) 6809.
[70] J.A. Joens, J. Chem. Phys. 100 (1993) 3407.
[71] J.A. Joens, J. Chem. Phys. 101 (1994) 5431.
[72] O. Bludsky, P. Jensen, Mol. Phys. 91 (1997) 653.
[73] K. Bogumil, J. Orphal, S. Voigt, H. Bovensmann, O.C. Fleischmann, M. Hartmann, T. Homann, P. Spietz, A. Vogel, J.P. Burrows, in: Proceedings of the 1st European Symposium on Atmospheric Measurements from Space, Vol. 2, ESA Earth Sciences Division, ESTEC, Noordwijk, 1999, p. 443.